

# Anisotropic Metamaterials as sensing devices in acoustics and electromagnetism

Jose Sánchez-Dehesa\*, Daniel Torrent, Jorge Carbonell

Wave Phenomena Group, Dept. Ingenieria Electronica, Universitat Politecnica de Valencia,  
Camino de Vera s/n, 46022 Valencia, SPAIN

## ABSTRACT

We analyze the properties of acoustic and electromagnetic metamaterials with anisotropic constitutive parameters. Particularly, we analyze the so-called Radial Wave Crystals, which are radially periodic structures verifying the Bloch theorem. This type of crystals can be designed and implemented in acoustics as well as in electromagnetism by using anisotropic metamaterials. In acoustics, we have previously predicted that they can be employed as acoustic cavities with huge quality factors and also like dynamically driven antennas. Similar functionalities are here proven in the electromagnetic domain with, in particular, an analysis of the functionality of practical devices operating in the microwave regime. Starting from our recent works on anisotropic structures and their comparison in both application fields, we present a complete discussion concerning their properties in acoustics and electromagnetics.

**Keywords:** metamaterials, anisotropic parameters, effective medium theory, acoustic waves, electromagnetic waves.

## 1. INTRODUCTION

During the last decade a huge research effort has concentrated on the possibility of controlling wave propagation phenomena based on the use of microstructured devices, usually termed as ‘metamaterials’<sup>1</sup>. This broad area of research covers aspects from theory of wave propagation in complex media to micro- and nano-fabrication techniques (with their corresponding operation frequencies), and even different disciplines or application fields like acoustics or electromagnetism. One of the core targets of this effort is related to the so-called ‘total control’ of wave propagation. Towards this goal a number of unusual phenomena have been investigated which in principle cannot be achieved with ‘natural’ materials: negative refraction, super-resolution focusing or cloaking<sup>2-4</sup>. On the foundations of this field is the use of artificial microstructures made of ‘small’ (as compared to the operation wavelengths) elements or inclusions as unitary constituents that possess a proper geometrical arrangement and characteristic parameters. They are usually, even though not necessarily, implemented with periodic and/or multilayered structures<sup>5</sup>. These devices operate in the ‘long-wavelength’ regime, where the operation wavelength is much larger than the characteristic dimensions of the unit cell elements. Additionally, one of the characteristic features in the background of some interesting phenomena, such as wave channeling and routing or magnification, is wave propagation anisotropy<sup>6</sup>. Anisotropic phenomena have been largely investigated both in acoustics<sup>7-9</sup> and electromagnetism<sup>10,11</sup>. Control of anisotropic propagation is a key condition to allow a number of applications, which can cover a broad spectrum of areas from directive antennas<sup>12</sup> to cloaking devices<sup>13,14</sup>. In this context, periodic, semi-periodic and/or multilayered microstructures, depending also on the desired spatial configuration (1D, 2D or 3D), have been studied to satisfy different types of targets. These studies are usually based on the analysis of the desired propagation characteristics at the macroscopic level, and of the elementary constituent cells at the microscopic level<sup>4,15,16</sup>. In particular, the selection of arrangement and unitary cell element is inherently linked to the targeted spatial configuration, wave polarization (for EM waves), operation frequency and dispersive characteristics, and isotropic or anisotropic behavior, among others. Macroscopic characteristics are usually described by effective constitutive parameters<sup>17-19</sup>, but also in design and engineering environments by equivalent circuit models<sup>20,21</sup>. This permits the analysis in terms of propagation characteristics (allowed or forbidden modes, propagation and attenuation constants...), that can be summarized for example in dispersion diagrams. Radial structures have also been investigated starting from dielectric photonic crystals<sup>5,22,23</sup> with the target of creating isotropic bandgaps and high-Q resonators<sup>24</sup>. Nevertheless, these radial proposals were not easily described in terms of purely periodic parameters.

\* jsdehesa@upvnet.upv.es; phone +34- 963879607; fax +34- 963877609; www.upv.es

In this paper, we analyze and compare the wave propagation characteristics of the so-called Radial Wave Crystals (RWC)<sup>5</sup>. This term or device category can be adapted to the field of acoustics as Radial Sonic Crystals (RSC) and to electromagnetic as Radial Photonic Crystals (RPC). These types of metamaterial-inspired microstructures have the original characteristic of being invariant under translation, by implementing radially dependent constitutive parameter functions in multilayered systems. Although they were first analyzed for acoustic waves<sup>5,25</sup> clear analogies can be established between both application fields<sup>26</sup>, that can confirm equivalent behaviors. For a 2D configuration, the fundamental characteristic of these microstructures derives from the periodicity of the radial profile of the constitutive parameters, which are anisotropic. In the following, this is first analyzed by means of the proper design equations, together with the dispersion diagram information and related propagation parameters. Then, moving to the more practical aspects and application potentiality, finite size structures based on these concepts are studied as resonating elements. Following, the excitation of RPC structures with line sources is assessed. Some potential applications are pointed out. Finally, a practical design of a sample microwave microstructure is performed taking into account some simplifications that allow the feasibility of the device. These limitations are imposed on the number of constitutive parameters and layers implemented. The paper ends with a conclusion section summarizing the main findings of this work.

## 2. RADIAL WAVE CRYSTALS FOR ACOUSTIC AND ELECTROMAGNETIC WAVES

### 2.1 Design equations

If we comparatively analyze the governing field equations in both application fields, we can see that an equivalent fundamental problem can be formulated. Focusing on 2D configurations, a RWC can be designed in such a way to satisfy the fundamental condition of being invariant under translation in cylindrical coordinates. Both problems share the wave nature of the respective solutions to a common tensor equation, i.e. the Helmholtz equation. It can be expressed in cylindrical coordinates for anisotropic media<sup>27</sup> respectively for acoustic (sound pressure) and electromagnetic (electric field) waves, where  $\omega$  is the angular frequency. For the radial part, we respectively have for acoustic<sup>5</sup> and electromagnetic<sup>28</sup> waves:

$$\left[ -\frac{B(r)}{r} \frac{\partial}{\partial r} \left( \frac{r}{\rho_r(r)} \frac{\partial}{\partial r} \right) + \frac{q^2 B(r)}{r^2 \rho_\theta(r)} \right] P_q(r) = \omega^2 P_q(r) \quad (1)$$

$$\left[ -\frac{1}{r \varepsilon_z(r)} \frac{\partial}{\partial r} \left( \frac{r}{\mu_\theta(r)} \frac{\partial}{\partial r} \right) + \frac{q^2}{r^2 \varepsilon_z(r) \mu_r(r)} \right] E_q(r) = \omega^2 E_q(r) \quad (2)$$

These equations can be subsequently adapted to each field type taking into account the necessary boundary conditions that hold. In equation (1),  $r/\rho_r(r)$ ,  $B(r)/r$  and  $r\rho_\theta(r)$  can be made simultaneously periodic by taking the appropriate parameter definition functions. At the same time, in equation (2) terms  $r/\mu_\theta(r)$  and  $r\mu_r(r)$  can also be made simultaneously periodic, together with  $r\varepsilon_z(r)$ , so the invariance under translation condition, as stated above, is possible. This development is translated to EM waves from the original acoustic scalar proposal<sup>5</sup>, and in this case it applies to TM<sup>z</sup> modes (E<sup>z</sup> modes) for the 2D case. With this configuration it is possible to apply Bloch's theorem to obtain a band structure for the radial equations.

An implementation of a RWC can be made, in both application fields, by using two alternating metamaterial layers of types  $a$  and  $b$  with constant thicknesses  $d_a$  and  $d_b$  along the radial direction ( $d = d_a + d_b$ ). We can introduce a notation with a vector containing the constituent parameter functions  $\mathbf{X}(r) = (\rho_r(r), \rho_\theta(r)^{-1}, B(r)) \equiv (\mu_r(r)^{-1}, \mu_\theta(r), \varepsilon_z(r)^{-1})$ , that, depending on the layer type ( $a$  or  $b$ ) and the radial coordinate  $r$ , can be expressed as:

$$\mathbf{X}(r) = \begin{cases} r \hat{\mathbf{X}}_a & \text{if } (n-1)d < r < (n-1)d + d_a \\ r \hat{\mathbf{X}}_b & \text{if } (n-1)d + d_a < r < nd \end{cases} \quad (3)$$

where  $n$  is an integer that takes values  $n = 1, 2, \dots, \infty$  and  $\hat{\mathbf{X}}_i$  (for  $i = a, b$ ) are (normalized) vectors whose components are real numbers giving the slope of the linearly dependent electromagnetic parameters, i.e.  $\hat{\mathbf{X}}_i = (\hat{\mu}_{ir}^{-1}, \hat{\mu}_{i\theta}, \hat{\varepsilon}_{iz}^{-1}) \equiv (\hat{\rho}_{ir}, \hat{\rho}_{i\theta}^{-1}, \hat{B}_i)$ . By introducing  $\hat{\mathbf{X}}(r)$  in equations (1) and (2), we obtain the 2D wave equations

for the respective layers ( $a$  and  $b$ ):

$$\frac{\partial^2 P_q(r)}{\partial r^2} + \left[ \omega^2 \frac{\hat{\rho}_{ir}}{\hat{B}_i} - q^2 \frac{\hat{\rho}_{ir}}{\hat{\rho}_{i\theta}} \right] P_q(r) = 0 \quad i = a, b \quad (4)$$

$$\frac{\partial^2 E_q(r)}{\partial r^2} + \left[ \omega^2 \hat{\epsilon}_{iz} \hat{\mu}_{i\theta} - q^2 \frac{\hat{\mu}_{i\theta}}{\hat{\mu}_{ir}} \right] E_q(r) = 0 \quad i = a, b \quad (5)$$

Both equations for each one of the layers  $a$  and  $b$  have plane-wave solutions with a dispersion relation given by:

$$k_{iq}^2 = \omega^2 \frac{\hat{\rho}_{ir}}{\hat{B}_i} - q^2 \frac{\hat{\rho}_{ir}}{\hat{\rho}_{i\theta}} \quad i = a, b \quad (6)$$

$$k_{iq}^2 = \omega^2 \hat{\epsilon}_{iz} \hat{\mu}_{i\theta} - q^2 \frac{\hat{\mu}_{i\theta}}{\hat{\mu}_{ir}} \quad i = a, b \quad (7)$$

Now, from equations (6) and (7) it is possible to obtain the dispersion relation for the multilayered structure by following a method similar to the one already employed in a previous reference<sup>29</sup>. The respective composite relations are given by:

$$\cos Kd = \cos k_{aq} d_a \cos k_{bq} d_b - \frac{1}{2} \left[ \frac{\hat{\rho}_{ar} k_{bq}}{\hat{\rho}_{br} k_{aq}} + \frac{\hat{\rho}_{br} k_{aq}}{\hat{\rho}_{ar} k_{bq}} \right] \sin k_{aq} d_a \sin k_{bq} d_b \quad (8)$$

$$\cos Kd = \cos k_{aq} d_a \cos k_{bq} d_b - \frac{1}{2} \left[ \frac{\hat{\mu}_{a\theta} k_{bq}}{\hat{\mu}_{b\theta} k_{aq}} + \frac{\hat{\mu}_{b\theta} k_{aq}}{\hat{\mu}_{a\theta} k_{bq}} \right] \sin k_{aq} d_a \sin k_{bq} d_b \quad (9)$$

where  $K$  is the Bloch wave number. These results imply that completely equivalent behaviors will be obtained for radial wave crystals in acoustics or electromagnetics if they are defined with equivalent constitutive parameters.

## 2.2 Effective constitutive parameters

Figure 1 displays the radial dispersion diagram for a RPC with constitutive parameters  $(\mu_{ra}^{-1}, \mu_{\theta a}, \epsilon_{za}^{-1}) \equiv (\rho_{ra}, \rho_{\theta a}^{-1}, B_a) = (0.347r/d, 0.08r/d, 0.143r/d)$  and  $(\mu_{rb}^{-1}, \mu_{\theta b}, \epsilon_{zb}^{-1}) \equiv (\rho_{rb}, \rho_{\theta b}^{-1}, B_b) = (0.5r/d, 0.04r/d, 0.1r/d)$ .

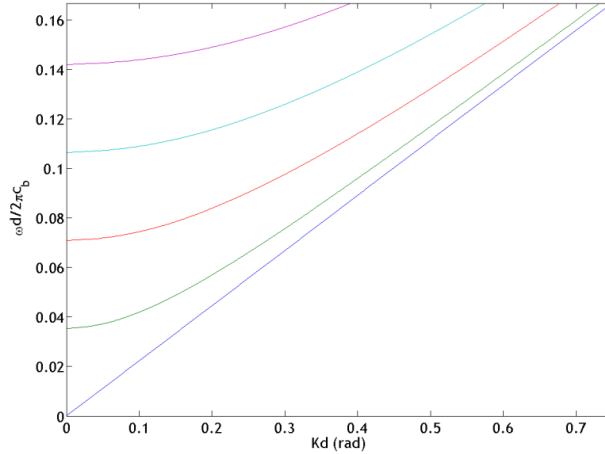


Figure 1. Dispersion diagram for the first 5 modes of a Radial Wave Crystal. The RWC is made from a multilayered structure of alternate layers of types  $a$  and  $b$  with constitutive parameters  $(\mu_{ra}^{-1}, \mu_{\theta a}, \epsilon_{za}^{-1}) \equiv (\rho_{ra}, \rho_{\theta a}^{-1}, B_a) = (0.347r/d, 0.08r/d, 0.143r/d)$  and  $(\mu_{rb}^{-1}, \mu_{\theta b}, \epsilon_{zb}^{-1}) \equiv (\rho_{rb}, \rho_{\theta b}^{-1}, B_b) = (0.5r/d, 0.04r/d, 0.1r/d)$  and periodicity parameter  $d = d_a + d_b$ .

The first 5 modes are included ( $q = 0, 1, 2, 3, 4$ ) for a microstructure with  $d = d_a + d_b$ . The layer dimensions directly fix the operation frequencies, so the structure is theoretically scalable at any frequency range. Modes with  $q > 0$  have a low frequency band gap with no transmission, and only the  $q = 0$  mode has no cutoff frequency. Designing a practical

structure based on this concept of RWC obviously requires a microstructure with a finite size, since the previous dispersion diagram analysis corresponds to the periodic unit cell. We have focused in the following on the electromagnetic version of the RWC, but as in the previous points, completely equivalent acoustic microstructures correspond to the electromagnetic ones described and analyzed in the following.

For a feasible Radial Photonic Crystal let us note that,  $\mu_r(r)$  and  $\varepsilon_z(r)$  reach unbounded values close to  $r = 0$ , and  $\mu_\theta(r)$  will follow a linear increase with  $r$ . These two considerations make that a practical implementation of a RPC will have a bounded shell shape (circular in our case), with a finite number of concentric layers and also a void (inner) cavity in its center. By taking the vector parameters  $\mathbf{X}(r)$  defined previously, a layer thickness of  $d_a = d_b = 5$  mm and an inner cavity radius of  $r_{int} = 15$  mm, we have generated the constitutive parameters corresponding to a 10 layers device (5 type  $a$  layers and 5 type  $b$  layers). They are displayed in Fig. 2. Curves for  $\mu_r(r)$ ,  $\mu_\theta(r)$ , and  $\varepsilon_z(r)$  are represented as a function of the radial distance from the center of the microstructure and in the area occupied by the RPC shell (15 to 65 mm radius). Let us note that the respective permittivity and permeability functions have stair-like shapes due to the fact that each parameter is alternating between layers  $a$  and  $b$  that follow the two linearly increasing (or inversely decreasing) functions of each layer type. Insets show 2D schemes of how the values of each parameter are distributed on the RPC shell surface with background values inside the inner (void) cavity and outside the shell border, where  $\varepsilon = \mu = 1$ . The values selected for the three parameters remain in any case within ranges that can be achieved with metamaterial-inspired unitary constituents based on micro-resonators and are positive.

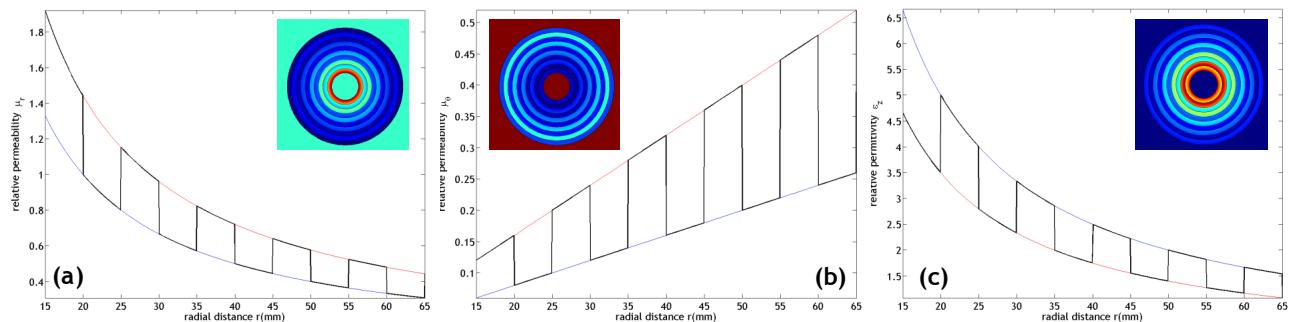


Figure 2. Constitutive parameter profiles for a 2D Radial Photonic Crystal with stair like shapes as a function of the radial coordinate  $r$  in the shell region. The origin of  $r$  is located at the center of the RPC. (a) radial permeability  $\mu_r$ ; (b) angular permeability  $\mu_\theta$ ; (c) permittivity  $\varepsilon_z$ . Actual parameter values (black curve) correspond to data in Fig. 1, and are bounded by the functions describing the parameter in the alternative layers of types  $a$  (red curve) and  $b$  (blue curve). Insets are color plots of the curve values in the device plane, high values correspond to red color and low values correspond to blue color.

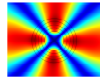
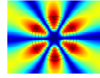
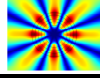
### 2.3 Resonant Radial Wave Crystal Shells

Once a finite size microstructure is considered for practical purposes, first application analyzed for the isolated structure is a resonator. RWC microstructures were studied as acoustic resonators<sup>25</sup>, by evaluating the resonance patterns and their characteristics. Here, in order to have a numerical verification of the theoretical formulation of previous section, we have used an electromagnetic commercial software package based on finite elements<sup>30</sup> to compute the resonant frequencies (eigen-frequencies) of a 4 layers RPC device. The constitutive parameters of this device are taken from those given in Fig. 2, where the parameters curves are truncated at 4 layers. The resonant device has in this case an inner radius  $r_{int} = 15$  mm and an external radius  $r_{ext} = 35$  mm.

Table 1 displays the resonant mode patterns, mode symmetries and resonant frequencies of all resonant modes in the frequency range from 2.5 GHz to 5 GHz. This range corresponds to the upper half of the frequency axis of the dispersion diagram of Figure 1. On the one hand, exact resonance frequencies are here determined by the finite size of the RPC shell which is 4 layers thick. On the other hand, frequency ranges where it is possible to observe each symmetry type are driven by the dispersion diagram of the infinite structure (see Fig. 1 where frequencies are normalized and correspond to the range from 0 to 5 GHz). Comparing the resonant frequencies of each mode and symmetry pattern with the corresponding branches in the dispersion diagram of Fig. 1, it is possible to confirm the co-existence of mode  $q = 0$  with the rest up to  $q = 4$ . Also, the obtained resonant mode patterns are in each occasion occurring above the cut off frequency

of the respective mode. These shell resonances are based on Bragg effects caused by the finite size of the microstructure in terms of radial and angular dimensions.

Table 1. Resonant frequencies for a 4 layers Radial Photonic Crystal between 2.5 and 5 GHz. Cut off frequencies calculated from the dispersion diagram of Figure 1 are also reported.

Mode pattern	Mode symmetry	$f_r$ (GHz)	Reduced profile RPC $f_{co}$ (GHz)
	shell Bragg $q = 2$ $m = 1$	2.89	1.06
	shell Bragg $q = 3$ $m = 1$	3.90	2.13
	shell Bragg $q = 4$ $m = 1$	4.94	3.19

### 3. COMBINATION WITH RADIATION SOURCES

In a further step, we have studied the interaction of line sources when they are combined with RPC microstructures and they illuminate them. As we are studying 2D configurations, a point source in the 2D plane is assimilated to a vertically oriented line source, i.e. parallel to the  $z$ -axis in the  $(r, \theta, z)$  coordinate system. A normalized source of 1A current is used for all cases in the following. The simulation domains are bounded with radiation boundaries, allowing radiation towards the outside.

Numerical results obtained with the full-wave solver have been obtained in several configurations, where the combination of the source and the RPC exhibits substantially different conceptual behaviors. In our case, we have basically evaluated the interaction between both elements in two situations. First possibility is to analyze the interaction with the line source when it is located inside the inner cavity, and illuminates the device at a resonance frequency of the RPC shell (Bragg resonance). Second possibility is illuminating the RPC externally with the line source located at a distance larger than  $r_{ext}$  from the center of the microstructure. An example of each one of these configurations is displayed in Fig. 3. These are plots of the E-field complex magnitude with a line source illuminating a 4 layers RPC microstructure with  $r_{int} = 15$  mm and  $r_{ext} = 35$  mm. In Fig. 3(a), the line source is located at a position  $x_a = 11$  mm,  $y_a = 0$  mm, i.e. within the inner cavity of the RPC (origin of coordinates is at the RPC center). In Fig. 3(b), the line source is located at a position  $x_b = y_b = 75$  mm. In both plots, the line sources excite the RPC at a frequency  $f = 3.90$  GHz. According to Table I, this frequency corresponds to a Bragg resonance associated to a  $q = 3$  symmetry resonant mode.

Figure 3(a), clearly proves that if the source frequency corresponds to a Bragg shell resonance, the shell strongly modifies the radiation pattern of the line source. Instead of having an omni-directional radiation pattern, it is changed to a sextupolar pattern matching the mode symmetry of the device. This is a powerful tool to tailor the radiation pattern of omni-directional sources to different shapes according to the mode distribution of the RPC shell. The radiation patterns will have a frequency dependent behavior, closely driven by the symmetry of the shell resonance patterns. Simulation results show that, due to the symmetry of the  $q > 0$  modes, it is not possible to excite them with a line source if this line source is located exactly at the center of the inner cavity. This is the reason why the line source is displaced with respect to the center in Fig. 3(a). Note also that the displaced position of the source with respect to the inner cavity center defines the maximum radiation directions of the combination shell plus source. Additional studies can be made on how the position of the line source in the central cavity is determinant to optimize the radiation properties of the combined source and shell. It is anyway anticipated that because the RPC is a “very ordered” system, radiated power of the combined system could be increased with respect to the isolated line source, as in other metamaterial combinations with radiating elements<sup>31,32</sup>. This type of analysis is out of the scope of this paper.

Figure 3(b) displays an interaction example of an external line source in close proximity to the RPC shell. It is again the same source frequency  $f = 3.90$  GHz. Within the RPC shell the E-field pattern associated to the  $q = 3$  mode is clearly excited. It is therefore possible to transfer energy from the source to the RPC taking advantage of the fact that it can trap it at the frequencies of the shell Bragg modes. At the same time, the resonance pattern excited in the shell is a proof of what frequency is being emitted by the external source. An additional interesting point with respect to this configuration

is the fact that the symmetric mode pattern of the E-field in the device is pointing towards the source. This resonance pattern is oriented towards the position of the external excitation source. This opens the possibility of assessing not only the frequency at which the source is emitting, but also the position from where it is emitting.

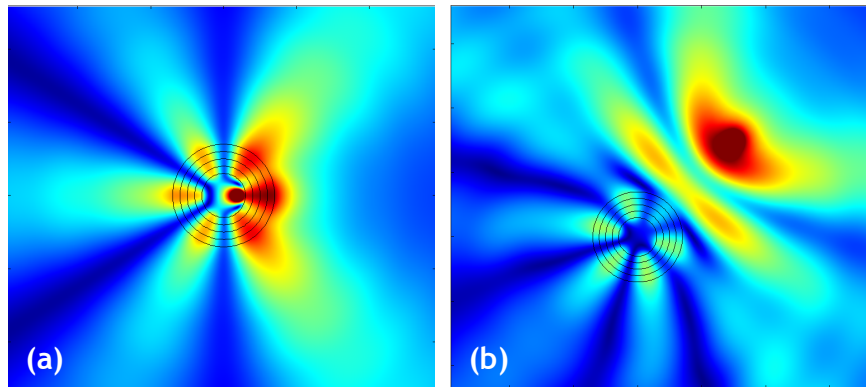


Figure 3. E-field magnitude plot for a 4 layers RPC device illuminated by a line source; (a) line source located at position  $x_a = 11$  mm  $y_a = 0$  mm from the RPC center, i.e. inside the central cavity; (b) line source located at position  $x_b = y_b = 75$  mm from the RPC center, i.e. external illumination. In both cases the line source emits at  $f = 3.90$  GHz, corresponding to a  $q = 3$  symmetry resonant mode.

An example to illustrate the potential application of RPCs as position sensors is given in Fig. 4. The E-field pattern of a line source illuminating a pair of identical RPC shells is depicted. Panel (a) represents the real part of the E-field, while panel (b) represents the magnitude of  $E^z$ . The source is located at a distance of 200 mm from each RPC center and radiates at a frequency  $f = 3.90$  GHz. This frequency corresponds to the resonance frequency of the  $q = 3$  symmetry mode (from Table I). Note in this case that the symmetric mode patterns of each RPC point towards the location of the illuminating source. Especially if the symmetry of the resonant mode is  $q = 1$ , only two RPCs could locate the exact position of a line source according to the orientation of the E-field maxima in the respective shells. If the RPCs are close one to the other, a second order interaction between them can happen: reflected wave from one RPC exciting the second RPC. This may limit the accuracy of the position sensing application.

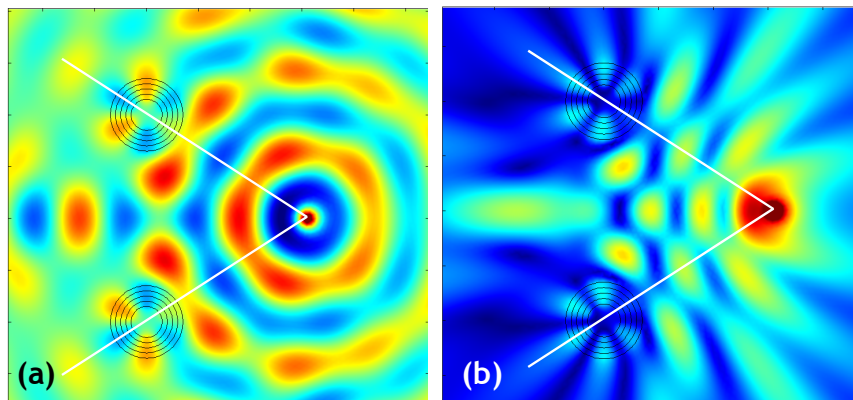


Figure 4. Field plots in (a) real part of the  $E^z$  component, in (b) magnitude of the E-field. Two identical RPC shells are illuminated by an external point source located at 200 mm of each RPC center. Source frequency is  $f = 3.9$  GHz, a  $q = 3$  resonance is excited in both shells. White lines are guides for the eye indicating that the main lobes are oriented and pointing towards the position of the excitation source.

#### 4. REDUCED RADIAL PHOTONIC CRYSTAL IMPLEMENTATION

It is possible to find an approximate equivalence between two devices of the same dimensions but with different parameter profile definitions. In particular, we have studied a reduced complexity shell, where only a  $\mu_\theta(r)$  profile is implemented, that can be compared to the previous full profile RPC, where all three constitutive parameters are implemented. Both devices should have the same size and number of layers for this purpose.



#### 4.1 Resonant Radial Wave Crystal Shells

For a practical implementation of the profile we have selected a unitary cell composed of a resonant split ring resonator (SRR) particle<sup>33</sup>. This unitary component has reduced bianisotropy effects compared for example with other SRRs<sup>34</sup>. This is important due to the fact that it is not desired that the array of resonators implementing the  $\mu_\theta(r)$  function interferes with the  $\mu_r(r)$  function (which in our case should be neutral  $\mu_r(r) = 1$ ). General permeability of an array of SRRs follows a Lorentz-like model with the resonant frequency separating positive and negative values of effective permeability<sup>35</sup>. With the proper design of the geometric dimensions of the SRRs it is possible to define the permeability response at a specific frequency (the design frequency). An optimization process is required to match the desired permeability and permittivity values at the desired operation frequency. It is well known that for SRRs losses exist and are especially important for the frequencies close to the resonance frequency (due to the Lorentz-like model). This is especially critical when negative permeability values need to be implemented. Nevertheless, the proposed design (see Fig. 2) uses values of  $\mu_\theta(r)$  that are positive and below 1. It is possible to take advantage of a permeability range (in the Lorentz model) where the frequency dispersion is not as high as near the resonance frequency of the SRRs. At the same time, this makes that losses are reduced for the SRR response, with respect to other applications. Anyway, material losses derived from the use of copper and the dielectric material substrate are unavoidable.

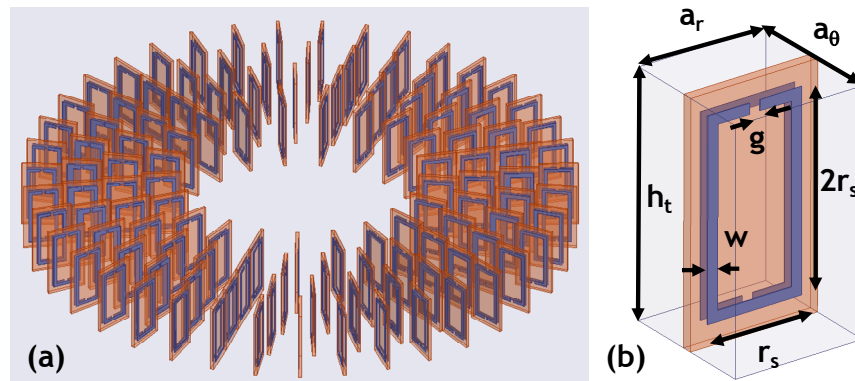


Figure 5. Reduced model implementation of a four layers simplified microstructure. Radially oriented SRRs implement the  $\mu_\theta(r)$  profile as in Fig. 2. (a) 4 layers microstructure with internal cavity radius  $r_{int} = 15$  mm and an integer number of Split Ring Resonators (SRRs) per layer; (b) SRR unit cell configuration with design parameters.

Figure 5 gives a schematic of the implemented design, together with the main characteristic dimensions. Figures 5(a) shows an oblique view of the RPC microstructure implemented through 4 concentric layers of SRRs. Each layer is ‘homogeneous’ (i.e. all SRRs forming one layer are identical) and implements the specific set of constitutive parameter values of Table IV. Basically, the values of  $\mu_\theta(r)$  and  $\epsilon_z = 3.4$  are reproduced for each designed layer. Also, this design is based on having an integer number of SRRs per layer and a constant angular separation between adjacent SRRs of the same layer (angular periodicity  $a_\theta$ ). The relationship between both parameters is  $a_\theta = \pi/3 \times a_r$ , guaranteeing that every concentric layer has six SRRs in addition to the previous one (cf. Table IV). Each circumference of the reported mean radiuses (17.5 to 32.5 mm) contains an integer number of equally spaced SRRs with angular periodicity  $a_\theta$ . Figure 5(b) displays the actual simulation scheme employed to extract the constitutive parameters of one unitary cell. It is composed of a broadside coupled SRR<sup>33</sup>, basically formed by two metallic and symmetric split rings patterned on both sides of dielectric plate. Dielectric material is Neltec 9220 of low permittivity and low loss ( $\epsilon_r = 2.2$  and  $\tan \delta = 0.0009$ ). Note that periodic boundary conditions mimic the presence of a complete array of identical elements with the corresponding periodicity constant (in this case  $a_\theta$  for the angular permeability). The constitutive parameters have been extracted using a standard Nicolson-Ross-Weir procedure<sup>17</sup>. These extracted parameters are also given in Table 2, together with the relative difference with respect to the target parameters. These differences are in general lower than 1%, a value comparable to the convergence accuracy in the numerical simulations. The unit cell has been simulated taking into account both possible incidence directions (with respective periodicity parameters  $a_r$  and  $a_\theta$ ). Although it is a Cartesian unit cell, it is assumed that it reproduces accurately the extracted parameters in cylindrical coordinates. This agreement is obviously better for the largest radius layers.

Table 2. Design parameters for the reduced 4 layers RPC. Inner cavity of size  $r_{int} = 15$  mm and an external shell radius  $r_{ext} = 35$  mm. Extracted parameters from numerical unit cell simulations are given with relative difference with respect to the target parameters

Design parameter (mm)	Layer #			
	1 (1a)	2 (1b)	3 (2a)	4 (2b)
$a_r$	5	5	5	5
$a_\theta$	5.236	5.236	5.236	5.236
$h_i$	9	9	9	9
$r_s$	3.7	3.7	3.7	3.7
$w$	0.4	0.4	0.6	0.4
$g$	0.42	0.6	0.24	0.41
mean radius	17.5	22.5	27.5	32.5
# rings/layer	21	27	33	39
Extracted parameters				
$\mu_\theta$	0.1434 (-0.76%)	0.0974 (0.10%)	0.2481 (0.24%)	0.1468 (-0.34%)
$\varepsilon_z$	3.4137 (0.40%)	3.4087 (0.26%)	3.4350 (1.03%)	3.4148 (0.44%)

## 4.2 Resonant Radial Wave Crystal Shells

The analysis of the reduced parameter set prototype has been performed in two parallel ways, allowing to compare the obtained results and to validate the functionality of the designed microstructure.

In a first approach, the reduced profile shell has been numerically studied by defining analytically the anisotropic material forming each one of the four layers. This is a 2D simulation where the parameter functions in Fig. 2 are directly assigned to the multilayer domains of the finite element solver<sup>30</sup>. The study of the resonant modes of this microstructure was summarized in Table 1. We have therefore selected a  $q = 3$  symmetry (sextupolar) mode pattern that resonates at  $f = 3.90$  GHz, and used it as our design frequency. The fact of having only four layers thickness (instead of ten reported in Fig. 2) limits the order and number of the shell Bragg resonances. Let us also mention that at this operation frequency, free space wavelength is  $\lambda(3.90 \text{ GHz}) = 77$  mm, which is much larger than the layer thickness  $d_a = d_b = 5$  mm.

Second approach consisted of implementing, at the selected resonant frequency ( $f = 3.90$  GHz), the RPC microstructure but based in a SRR configuration as depicted in Fig. 5. A layer by layer design is performed by optimizing each device unit cell as it was illustrated in Table 2. Then, the complete structure is numerically analyzed with a different 3D finite element solver<sup>36</sup>. It is based on the simulation of discrete SRR resonators to implement the designed geometry instead of defining the RPC directly from analytical equations for the constitutive parameters. The ab-initio simulations have been performed only at the design frequency 3.90 GHz because of the computational resources required, but the results should be close to what is expected in a measurement setup at this frequency. Let us recall that this microstructure is designed for  $\text{TM}^z$  polarization. The 3D simulation domain, if it has to be compared to the 2D simulation results of the first approach, is bounded on the  $z$ -axis by Perfect Electric Conductor (PEC) boundaries. Therefore, this configuration mimics a  $z$ -invariant simulation domain. One important note about this second approach is the fact that the SRR behavior is inherently dispersive, with a Lorentz-like function for each array of elements in the multilayers. This makes that the values of both  $\mu_\theta$  and  $\varepsilon_z$  are valid only in a frequency range close to the design frequency. On the one hand, it is a bandwidth limited approach, but on the other hand, the selected values of  $\mu_\theta$  and  $\varepsilon_z$  are not close to the highly dispersive values obtained near the resonance frequency of the SRRs (i.e.  $\mu_\theta$  and  $\varepsilon_z$  have smooth variations around the design frequency).

We intend to verify the interaction of a line source in close location with respect to the RPC. The complex E-field magnitude patterns in the region around the RPC are displayed in Fig. 6. The RPC is centered on the origin of the radial coordinate system and the line source is located at position  $x_0 = -40$  mm  $y_0 = 40$  mm. Figure 6(a) shows the result for an analytical model simulation and Fig. 6(b) shows the result for the SRR implemented RPC (cut plane plot of the 3D simulation). Color scale represents E-field magnitude with same range in both plots. From this comparison, it is clear that the  $q = 3$  mode is excited in the RPC shell at the predicted resonance frequency,  $f = 3.90$  GHz. Field maxima and minima are closely comparable in both simulations and orientation of the mode pattern towards the source is preserved.



Within the RPC shell, the dielectric plates between the metallic tracks of the SRRs concentrate large amounts of electric field, but overall the field patterns closely follow the ‘envelope’ corresponding to the  $q = 3$  field pattern.

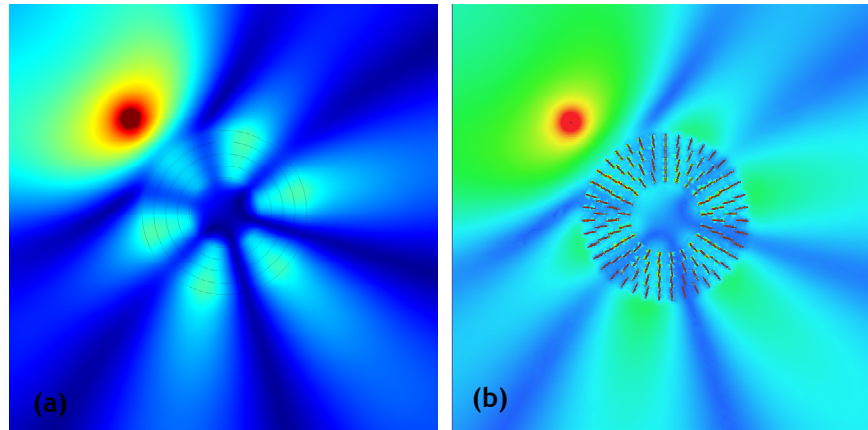


Figure 6. E-field magnitude plots of an external line source exciting the  $q = 3$  resonance of a simplified RPC at  $f = 3.90$  GHz. (a) full wave simulation from an analytical definition of the constitutive parameters; (b) full wave (ab-initio) simulation of the reduced model implementation on an horizontal cut plane. Resonance pattern associated to the  $q = 3$  mode is apparent in both results inside and outside the RPC shell.

## 5. CONCLUSIONS

An in depth analysis has been performed on Radial Photonic Crystal microstructures that can be basically described as radially periodic media that verify Bloch’s theorem. They are implemented with dependent constitutive parameters that make them systems with unique characteristics. These ‘very ordered’ microstructures have been analyzed starting from their ideal or full profile configuration and showing their possible application as resonant structures. Their combination with radiation sources allows the analysis of the interactions by pointing out possible applications as beam-forming shells for line sources. Their application as frequency and position sensors is outlined and explicitly demonstrated with a simulation example. Also, in view of a practical implementation, a reduced parameter profile model has been investigated. It is showed that it is possible to retain a great part of the RPC functionality even if the complexity of the device is hence affordable in terms of standard fabrication techniques. Some ab-initio simulations demonstrate that the RPC can be implemented in practice by using split ring resonator arrangements. In particular, a multilayered microstructure synthesizing a radially dependent angular permeability has been designed and compared to the analytical model. Results have been obtained in this case for the interaction with a line source and a plane wave. This study opens the path to further works on both analysis of specific RPC designs and fabrication and measurement of a RPC prototype.

## ACKNOWLEDGEMENTS

This work was supported in part by the Spanish Ministry of Science MICINN under Grants TEC 2010-19751 and Consolider CSD2008-00066 and by the U.S. Office of Naval Research under Grant N000140910554.

## REFERENCES

- [1] Engheta, N., and Ziolkowski, R. W., [Metamaterials: Physics and engineering explorations], Wiley-IEEE Press (2006).
- [2] Pendry, J. B., Schurig, D., and Smith, D. R., “Controlling electromagnetic fields,” *Science* 312, 1780 (2006).
- [3] Pendry, J. B., “Negative refraction makes a perfect lens,” *Phys. Rev. Lett.* 85, 3966 (2000).
- [4] Schurig, D., Mock, J. J., Justice, B. J., Cummer, S. A., Pendry, J. B., Starr, A. F., and Smith, D. R., “Metamaterial electromagnetic cloak at microwave frequencies,” *Science* 314, 977 (2006).

- [5] Torrent, D., and Sanchez-Dehesa, J., "Radial Wave Crystals: Radially Periodic Structures from Anisotropic Metamaterials for Engineering Acoustic or Electromagnetic Waves," *Phys. Rev. Lett.* 103, 064301 (2009).
- [6] Jacob, Z., Alekseyev, L. V., and Narimanov, E., "Optical hyperlens: Far-field imaging beyond the diffraction limit," *Optics Express* 14, 8247 (2006).
- [7] Bradley, C. E., "Time-Harmonic Acoustic Bloch Wave-Propagation in Periodic Wave-Guides .1. Theory," *J. Acoust. Soc. Am.* 96, 1844 (1994).
- [8] Bradley, C. E., "Time-Harmonic Acoustic Bloch Wave-Propagation in Periodic Wave-Guides .2. Experiment," *J. Acoust. Soc. Am.* 96, 1854 (1994).
- [9] Schoenberg, M., and Sen, P. N., "Properties of a Periodically Stratified Acoustic Half-Space and its Relation to a Biot Fluid," *J. Acoust. Soc. Am.* 73, 61 (1983).
- [10] Peng, L., Ran, L., and Mortensen, N. A., "Achieving anisotropy in metamaterials made of dielectric cylindrical rods," *Appl. Phys. Lett.* 96, 241108 (2010).
- [11] Carbonell, J., Cervera, F., Sanchez-Dehesa, J., Arriaga, J., Gumen, L., and Krokhin, A., "Homogenization of two-dimensional anisotropic dissipative photonic crystal," *Appl. Phys. Lett.* 97, 231122 (2010).
- [12] Valero-Nogueira, A., Alfonso, E., Herranz, J. I., and Baquero, M., "Planar slot-array antenna fed by an oversized quasi-TEM waveguide," *Microwave Opt Technol Lett* 49, 1875 (2007).
- [13] Ni, Y., Gao, L., and Qiu, C., "Achieving Invisibility of Homogeneous Cylindrically Anisotropic Cylinders," *Plasmonics* 5, 251 (2010).
- [14] Huang, Y., Feng, Y., and Jiang, T., "Electromagnetic cloaking by layered structure of homogeneous isotropic materials," *Optics Express* 15, 11133 (2007).
- [15] Cheng, Q., Cui, T. J., Jiang, W. X. and Cai, B. G., "An omnidirectional electromagnetic absorber made of metamaterials," *New Journal of Physics* 12, 063006 (2010).
- [16] Zhang, F., Potet, S., Carbonell, J., Lheurette, E., Vanbesien, O., Zhao, X. and Lippens, D., "Negative-Zero-Positive Refractive Index in a Prism-Like Omega-Type Metamaterial," *IEEE Trans. Microwave Theory Tech.* 56, 2566-2573 (2008).
- [17] Smith, D. R., Vier, D. C., Koschny, T. and Soukoulis, C. M., "Electromagnetic parameter retrieval from inhomogeneous metamaterials," *Physical Review E* 71, 036617 (2005).
- [18] Chen, X., Grzegorzczak, T., Wu, B., Pacheco, J. and Kong, J., "Robust method to retrieve the constitutive effective parameters of metamaterials," *Physical Review E* 70, 016608 (2004).
- [19] Szabo, Z., Park, G., Hedge, R., and Li, E., "A Unique Extraction of Metamaterial Parameters Based on Kramers-Kronig Relationship," *IEEE Trans. Microwave Theory Tech.* 58, 2646-2653 (2010).
- [20] Baena, J., Bonache, J., Martin, F., Sillero, R., Falcone, F., Lopetegi, T., Laso, M., Garcia-Garcia, J., Gil, I., Portillo, M., and Sorolla, M., "Equivalent-circuit models for split-ring resonators and complementary split-ring resonators coupled to planar transmission lines," *IEEE Trans. Microwave Theory Tech.* 53, 1451-1461 (2005).
- [21] Rogla, L. J., Carbonell, J. and Boria, V. E., "Study of equivalent circuits for open-ring and split-ring resonators in coplanar waveguide technology," *IET Microwaves Antennas & Propagation* 1, 170-176 (2007).
- [22] Horiuchi, N., Segawa, Y., Nozokido, T., Mizuno, K. and Miyazaki, H., "Isotropic photonic gaps in a circular photonic crystal," *Opt. Lett.* 29, 1084-1086 (2004).
- [23] Horiuchi, N., Segawa, Y., Nozokido, T., Mizuno, K. and Miyazaki, H., "High-transmission waveguide with a small radius of curvature at a bend fabricated by use of a circular photonic crystal," *Opt. Lett.* 30, 973-975 (2005).
- [24] Xiao, S. and Qiu, M., "High-Q microcavities realized in a circular photonic crystal slab," *Photonics and Nanostructures-Fundamentals and Applications* 3, 134-138 (2005).
- [25] Torrent, D. and Sanchez-Dehesa, J., "Acoustic resonances in two-dimensional radial sonic crystal shells," *New Journal of Physics* 12, 073034 (2010).
- [26] Carbonell, J., D. Torrent, Diaz-Rubio, A. and Sanchez-Dehesa, J., "Multidisciplinary approach to cylindrical anisotropic metamaterials," *New J. Phys.* 13, 103034 (2011).
- [27] Chew, W., [Waves and fields in inhomogeneous media], Wiley-IEEE Press, New York (1999).
- [28] Harrington, R. F., [Time-Harmonic Electromagnetic Fields], New York, NY: IEEE Press - Wiley Interscience (1961).
- [29] Brekhovskikh, L. M., and Beyer, R. T., [Waves in Layered Media], New York, NY, Academic Press New York (1980).
- [30] Comsol AB (Sweden), "Comsol Multiphysics (v. 4.1)," (2010).

- [31] Arslanagic, S., Ziolkowski, R. W., and Breinbjerg, O., "Analytical and numerical investigation of the radiation from concentric metamaterial spheres excited by an electric Hertzian dipole," *Radio Sci.*, 42, RS6S16 (2007).
- [32] Arslanagic, S., Ziolkowski, R. W., and Breinbjerg, O., "Excitation of an electrically small metamaterial-coated cylinder by an arbitrarily located line source," *Microwave Opt. Technol. Lett.* 48, 2598-2606 (2006).
- [33] Marques, R., Medina, F., and Ruffini-El-Idrissi, R., "Role of bianisotropy in negative permeability and left-handed metamaterials," *Physical Review B* 65, 144440 (2002).
- [34] Pendry, J. B., Holden, A. J., Robbins, D. J., and Stewart, W. J., "Magnetism from conductors and enhanced nonlinear phenomena," *IEEE Trans. Microwave Theory Tech.* 47, 2075-2084 (1999).
- [35] Carbonell, J., Rogla, L. J., Boria, V. E., and Lippens, D., "Design and experimental verification of backward-wave propagation in periodic waveguide structures," *IEEE Trans. Microwave Theory Tech.* 54, 1527-1533 (2006).
- [36] Ansoft, "High Frequency Structure Simulator (HFSS), v.13," (2011).